

# Hidden Synaptic Structures Control Collective Network Dynamics

Lorenzo Tiberi<sup>1,2</sup>, David Dahmen<sup>1</sup>, and Moritz Helias<sup>1,2</sup>

<sup>1</sup>*Institute of Neuroscience and Medicine (INM-6) and Institute for Advanced Simulation (IAS-6) and JARA-Institute Brain Structure-Function Relationships (INM-10), Jülich Research Centre, Jülich, Germany and*

<sup>2</sup>*Institute for Theoretical Solid State Physics, RWTH Aachen University, 52074 Aachen, Germany*

A common approach to model local neural circuits is to assume random connectivity. But how is our choice of randomness informed by known network properties? And how does it affect the network's behavior? Previous approaches have focused on prescribing increasingly sophisticated statistics of synaptic strengths and motifs. However, at the same time experimental data on parallel dynamics of neurons is readily accessible. We therefore propose a complementary approach, specifying connectivity in the space that directly controls the dynamics – the space of eigenmodes. We develop a theory for a novel ensemble of large random matrices, whose eigenvalue distribution can be chosen arbitrarily. We show analytically how varying such distribution induces a diverse range of collective network behaviors, including power laws that characterize the dimensionality, principal components spectrum, autocorrelation, and autoresponse of neuronal activity. The power-law exponents are controlled by the density of nearly critical eigenvalues, and provide a minimal and robust measure to directly link observable dynamics and connectivity. The density of nearly critical modes also characterizes a transition from high to low dimensional dynamics, while their maximum oscillation frequency determines a transition from an exponential to power-law decay in time of the correlation and response functions. We prove that the wide range of dynamical behaviors resulting from the proposed connectivity ensemble is caused by structures that are invisible to a motif analysis. Their presence is captured by motifs appearing with vanishingly small probability in the number of neurons. Only reciprocal motifs occur with finite probability. In other words, a motif analysis can be blind to synaptic structures controlling the dynamics, which instead become apparent in the space of eigenmode statistics.

Random matrices have been employed to describe the most disparate physical systems [1, 2], starting from nuclear energy levels in the 1950s [3]. Also in models of local cortical circuits, synaptic variability is often described as a random connectivity matrix [4–7]. Differently than typical physical systems, however, neural networks can learn their interaction structure: Through plasticity, synapses can organize into *ad hoc* configurations to perform specific computational tasks. It is therefore important to carefully ask how a neural network's function informs and constrains synaptic statistics. How do different choices of random connectivity affect the network behavior? And how is such choice informed by experimental evidence?

A common approach is to specify certain synaptic statistics [8, 9] based on experimental data on synaptic strengths and motifs [10]. Still, there is another large, if not prevalent, part of experiments which focuses on the parallel dynamics of neurons, rather than their microcircuitry. Neuronal activity is typically analyzed with regard to dynamical properties such as its relaxation [11–13], correlations [14], dimensionality [15–17], and principal components spectrum [17]. These measures of a network's function could be used to infer the underlying connectivity. For example, the aforementioned quantities are ubiquitously found to follow power laws: their exponents could be minimal and robust parameters linking observed dynamics and connectivity. In general, a theoretical framework is needed that directly links measures of network dynamics to connectivity parameters. To this end, we propose a novel approach, which specifies connectivity in the space that directly controls the dynamics

– the space of eigenmodes (Fig. 1).

We develop a theory for a novel ensemble of large random matrices, whose eigenvalue distribution can be chosen arbitrarily. We show how the shape of the eigenvalue distribution directly controls the power-law exponents characterizing the dynamical quantities listed above. Specifically, these are related to the exponent controlling the density of nearly-critical eigenvalues. Therefore, our theory provides a solid link between connectivity and observable neural dynamics. This can be used to inform connectivity choices when devising neural network models.

We show that, by varying the connectivity, a network can tune into a wide range of different behaviors: response and correlation functions transition from an exponential to a power-law decay in time (Fig. 3); neural activity transitions from high to low dimensional Fig. 4). Therefore, our largely extended ensemble of connectivity matrices allows to ask optimization questions. Which connectivity would a network learn in order to perform optimal computation? For example, we show how the appropriate connectivity choice can tune the principal components spectrum to have a power-law exponent, which is argued to be optimal for the encoding of natural image stimuli [17] (Fig. 5).

The typical *synaptic space approach* to connectivity derives the eigenmode statistics from some specified synaptic statistics. Our *dynamics space approach* proceeds in a specular manner (Fig. 1). From the statistics of eigenmodes we derive the corresponding synaptic statistics, finding a surprising result. At leading order in the number of neurons, only second order reciprocal motifs can

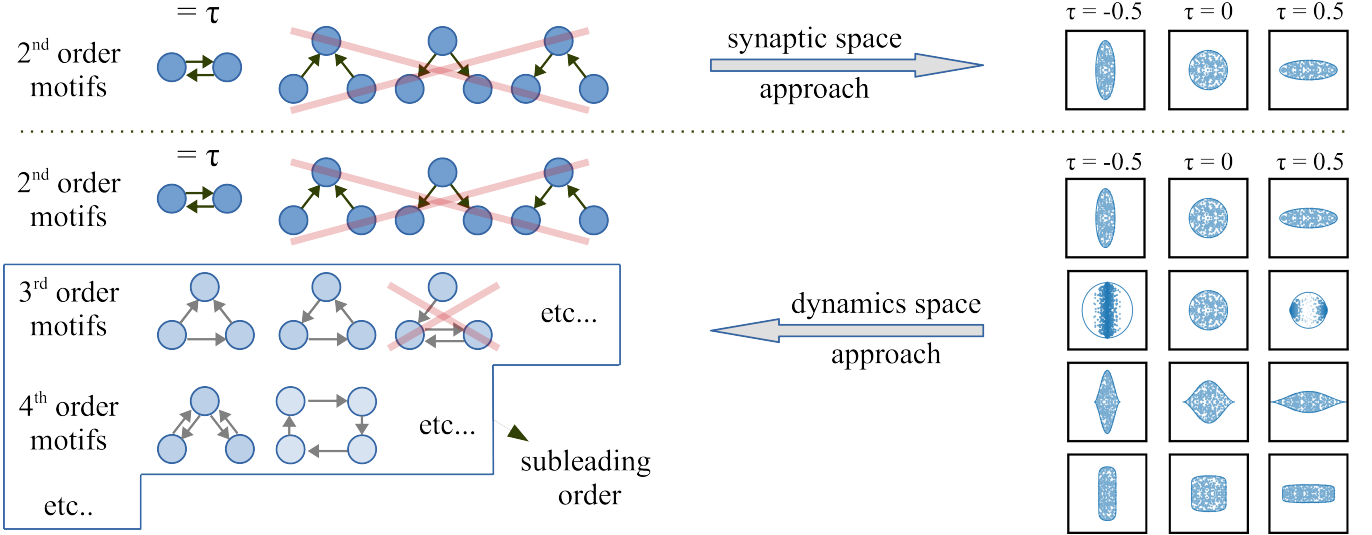


Figure 1. Schematic representation of the synaptic vs dynamics space approach. Top: synaptic space approach. Some motif statistics are assumed (left) and the eigenmode statistics (right) are derived. An archetypal approach assumes only the presence of second order reciprocal motifs. The corresponding eigenvalue distribution is uniform on an ellipse. Bottom: dynamics space approach. We specify the dynamics space statistics, allowing for any desired shape of the eigenvalue distribution (right). The derived synaptic statistics (left) predicts only reciprocal motifs to leading order, as in the archetypal approach. Higher order motif structures are present, but are subleading in the number of neurons.

be observed. These alone cannot account for the wide range of dynamical behaviors mentioned above. In fact, this is controlled by synaptic structures that are invisible to a motif analysis: In synaptic space, the presence of these structures is only captured by higher order motifs, appearing with vanishingly small probability in the number of neurons (Fig. 1). In dynamics space, instead, these structures are clearly reflected by the different eigenvalue distributions. In other words, a motif analysis would not distinguish between connectivities associated with very different dynamical behaviors (Fig. 2). This fact highlights the importance of complementing the synaptic space approach with a dynamics space point of view.

In Section I we introduce the network model here studied and the proposed random matrix ensemble. In Section II we characterize the effect of different eigenvalue distributions on the network dynamics. Specifically, we study the autocorrelation and autoresponse functions (IIA), the dimensionality (IIB) of neural activity, and its principal components spectrum (IIC). In Section III we discuss in more detail the synaptic statistics of our ensemble (IIIA and IIIC). We also numerically extend our results to the case of strongly non-orthogonal eigenvectors, as those appearing in random Gaussian matrices (IIIB). In the concluding Section IV we discuss the relevance of our work, in particular in relation with experimental recordings of neuronal dynamics.

## I. SETTING

We consider the recurrent network of linear rate neurons

$$\tau \partial_t x_i(t) = -x_i(t) + \sum_j J_{ij} x_j(t) + \xi_i(t), \quad (1)$$

where  $x_i(t)$  is the rate activity of neuron  $i$  at time  $t$ ;  $i = 1, \dots, N$ .  $J_{ij}$  describes the recurrent connection from neuron  $j$  to  $i$ .  $\tau$  is the characteristic timescale of neuronal response. The network is driven by Gaussian white noise  $\xi_i(t)$ , with zero mean and variance  $\langle \xi_i(t) \xi_j(t') \rangle = D \delta_{ij} \delta(t - t')$ . In the following, we consider Eq. (1) in dimensionless units, setting  $\tau = D = 1$ . In the linear regime, the second order statistics of various network models, comprising integrate-fire and inhomogeneous Poisson neurons, is well captured by Eq. (1) [18, 19]. In that case,  $J$  is an effective connectivity induced by the underlying model architecture.

Local neural circuits present strong variability in their connectivity. A common minimal approach is to model such variability as disorder, choosing  $J$  as a random matrix. Most likely, brain networks are not completely disordered: we expect them to have some function, thus some underlying connectivity structure. In the random connectivity setting, information about the network function or structure can be included in the model through the choice of statistics for the random connectivity  $J$ .

In previous works, the choice for the statistics of  $J$  has been inspired by the connectivity structure of brain networks. For example, various works [8, 9] have considered

connectivity motifs [10], that is the occurrence of certain subgraphs with higher chance than random. These can be modeled by a non-vanishing moment of the elements of  $J$  involved in the motif [9]. In an archetypal approach [4, 20], for example,  $J$  is assumed Gaussian with statistics

$$g^2 \equiv N \langle J_{ij}^2 \rangle \quad \tau \equiv \langle J_{ij} J_{ji} \rangle / \langle J_{ij}^2 \rangle, \quad i \neq j. \quad (2)$$

Only two parameters are present: the synaptic gain  $g$  models the overall strength of recurrent connections, while the degree of (anti)symmetry  $\tau$  controls correlations between reciprocal connections, which can be associated with an abundance of reciprocal motifs. Throughout the manuscript, we will refer to this connectivity choice as the archetypal choice for  $J$  and use it for comparison with our approach.

Rather than the network structure, in this work we want to use the network function, i.e. its dynamical behavior, to inform the choice of random  $J$ . Indeed, experimental data on parallel dynamics of neurons is more readily accessible than their microcircuitry. Furthermore, Eq. (1) represents an effective model of neuronal dynamics, rather than an accurate microscopic description of neural circuits. It is therefore natural to justify the choice of  $J$  as that of an effective connectivity, effectively reproducing some observed or desired collective dynamics.

The main idea of this work is to specify the statistics of  $J$  in the space that directly controls the network dynamics: the space of eigenmodes. We can always decompose  $J$  into its eigenvalues  $\lambda_\alpha$  and right eigenvectors  $V_\alpha$  as

$$J_{ij} = \sum_{\alpha=1}^N V_{i\alpha} \lambda_\alpha V_{\alpha j}^{-1} \quad (3)$$

Eigenvalues and eigenvectors have a direct dynamical interpretation: a linear combination of neurons  $\sum_i V_{\alpha i}^{-1} x_i$  represents a collective mode of neuronal activity, with dynamical response  $\propto \exp(-(1 - \lambda_\alpha)t)$ . Thus, calling an eigenvalue  $\lambda = \lambda_x + i\lambda_y$ , the associated mode has decay constant  $1 - \lambda_x$  and oscillation frequency  $\lambda_y$ . The distribution of eigenvalues associated with the connectivity  $J$  therefore characterizes the dynamical repertoire available to the network. In fact, its knowledge has already proven important in the archetypal approach. In that case, eigenvalues are uniformly distributed on a centered ellipse in the complex plane [20] (Fig. 1, top). The transition to chaos occurring in the nonlinear regime, for example, is well understood in terms of this ellipse crossing the line of linear instability,  $\lambda_x > 1$ .

Rather than the standard *synaptic space approach*, in which the eigenmode statistics are derived from some specified synaptic strengths statistics, here we take a specular, *dynamic space approach*, in which we define  $J$  through its eigenmode statistics, and later derive the corresponding synaptic strength statistics (Fig. 1). We define the eigenmode statistics as

$$\lambda \sim p(\lambda) \quad (4)$$

$$V = O + \nu G \quad (5)$$

Eq. (4) states that  $\lambda$  can be drawn from a distribution  $p$  of any arbitrary shape, provided its moments are bounded. One is therefore not constrained to a uniform elliptical distribution as in the archetypal approach, but can choose precisely what repertoire of decay constants and oscillation frequencies should be available to the network (see e.g. Fig. 1). In turn, we will show in Section II how the shape of  $p$  directly controls the dynamics, and thus it can be chosen according to the desired dynamical behavior of the network. The eigenvalues are drawn independently, following the same simplicity principle typically applied in the synaptic space approach, introducing minimal information in an otherwise disordered connectivity.

Following the same principle, we want to be agnostic regarding which direction a certain eigenmode takes in neuronal space. The eigenvector matrix  $V$  is therefore drawn independently from the eigenvalues. Eq. (5) defines it as a combination of a unitary and a complex Gaussian random matrix  $O$  and  $G$ , respectively, with interpolation parameter  $\nu \in [0, 1)$  controlling the degree of non-normality of the network. A precise definition of  $O$  and  $G$  can be found in A 1. Intuitively, varying  $\nu$  from 0 to 1 controls whether eigenmodes are orthogonal to each other ( $\nu = 0$ ), or can take on more and more random, overlapping directions ( $\nu \rightarrow 1$ ). The value  $\nu = 1$  is an upper limit at which eigenvectors are too overlapping and the synaptic gain  $g$  diverges (see Section III). A difference with the archetypal case of Gaussian  $J$  is that, there, eigenvalues and eigenvectors are found to be tightly correlated. This complicated correlation structure in eigenmode space emerges as a consequence of enforcing simple Gaussian statistics in synaptic space. Therefore, following the aforementioned simplicity principle, we do not want to assume such kind of correlations here. We explore this case numerically later in Section III. Further insights regarding our random matrix ensemble and differences compared to the archetypal approach are also discussed in Section III.

As we show in section Section II, varying the shape of the eigenvalue distribution causes a wide range of different dynamical behaviors. Surprisingly, however, we find this is not reflected by the leading order statistics of synaptic strengths. Just as for the archetypal connectivity, we find the synaptic strength statistics to be Gaussian, with only reciprocal motifs. In terms of the eigenmode statistics, the leading order synaptic strength statistics are given by

$$g^2 = \frac{1 + \nu^2}{1 - \nu^2} \left( \langle \lambda_x^2 \rangle_\lambda + \langle \lambda_y^2 \rangle_\lambda \right) \quad (6)$$

$$\tau = \frac{1 - \nu^2}{1 + \nu^2} \frac{\langle \lambda_x^2 \rangle_\lambda - \langle \lambda_y^2 \rangle_\lambda}{\langle \lambda_x^2 \rangle_\lambda + \langle \lambda_y^2 \rangle_\lambda} \quad (7)$$

where  $\langle \rangle_x$  denotes statistical averaging over the random variable  $x$ . Other second order motifs are absent. Higher order motifs are present, but only with a probability that

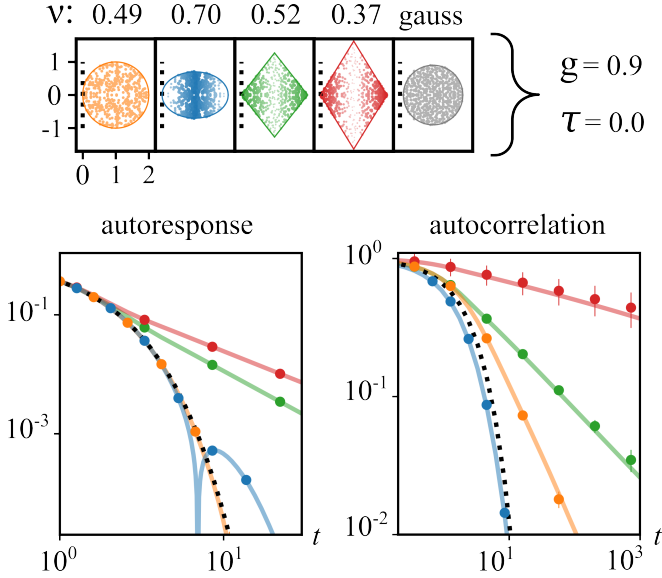


Figure 2. Same synaptic statistics correspond to different dynamics. Top: Various eigenmode distributions, sharing the same leading order synaptic statistics  $g = 0.9$ ,  $\tau = 0$ . The eigenvalue distribution in the complex plane  $k = 1 - \lambda$  is plotted and the degree of non-normality  $\nu$  is reported. The archetypal case of Gaussian  $J$  with the same statistics is also shown in black. Bottom: Autocorrelation and autoresponse functions, colored accordingly, show very different dynamics, decaying exponentially or with power-laws with various exponents. Lines: theory; markers: simulation; dotted, black line: known theory for the archetypal case of Gaussian  $J$ .

is vanishingly small in the number of neurons, and would thus be very hard if not impossible to detect experimentally. As a result, connectivities with the same leading order motif structure can correspond to different eigenmode distributions, thus to very different network dynamics, as exemplified in Fig. 2. In other words, the structure within a connectivity that causes a certain dynamical behavior may be invisible to an analysis of motif statistics, in the sense that it cannot be reduced to the generic abundance of certain connectivity patterns. In Section III we discuss in more detail the synaptic statistics of our ensemble.

## II. EFFECT ON DYNAMICS

In this section, we characterize how the eigenvalue distribution affects the network dynamics. It is natural to consider the shifted eigenvalues  $k \equiv \lambda - 1$ , that is the eigenvalues of the Jacobian  $J - \mathbb{I}$  of the dynamics. Thus, calling  $k \equiv k_x + ik_y$ , a mode has decay constant  $k_x$  and oscillation frequency  $k_y$ .

We will focus on systems at the edge of criticality, that is with eigenvalue distributions touching the line of linear instability  $k_x = 0$  from the right. Occasionally, we parameterize a small distance away from criticality by adding a small leak term  $-\delta \cdot x$  to the *rhs* of Eq. (1).

This effectively shifts the eigenvalues of the Jacobian  $k \rightarrow k + \delta$ , so the longest living modes have decay constant  $\delta$ , rather than 0. Moving away from criticality through  $\delta$  is equivalent to the more traditional rescaling of the spectral radius, through  $J \rightarrow (1 + \delta)^{-1} J$ , provided we also trivially rescale  $t \rightarrow (1 + \delta)t$  and  $D \rightarrow (1 + \delta)^{-1} D$  in Eq. (1). Here we use the former method, because  $\delta$  appears naturally as a mass term, in an analogy with classical critical phenomena exposed later.

Studying the nearly critical regime is of particular interest because of the wealth of characteristic features of criticality, like power-laws, that are experimentally observed in brain networks [13, 14, 17], feeding the so-called critical brain hypothesis [21]. Theoretical works also suggest the edge of criticality as an optimal computational regime [22, 23].

The main result of this section is that the density of nearly critical modes directly controls the power-law scaling exponents of various dynamical quantities: the population averaged autoresponse and autocorrelation function, the dimensionality of neural activity and the spectrum of its principal components. Precisely, we show these are controlled by either of the exponents  $d$  or  $\bar{d}$ , controlling the density of nearly critical modes through  $p(k_x) \stackrel{k \rightarrow 0}{\sim} k_x^{d-1}$  or  $p(\rho) \stackrel{k \rightarrow 0}{\sim} \rho^{\bar{d}-1}$ , where in the first case we consider approaching the critical point  $k = 0$  along the real axis  $k_x$ , while in the second case along the radial direction  $\rho$ , having called  $k \equiv \rho e^{i\phi}$ .

Close to criticality, the effect of the eigenvalue distribution on the dynamics is particularly apparent and can be quantified in terms of power-law exponents. However, we note that our theory is not restricted to nearly critical systems: also away from criticality, varying the eigenvalue distribution has similar qualitative effects.

### A. Autocorrelation and autoresponse

A common dynamical quantity considered in the study of disordered networks is the population averaged autocorrelation [4],  $A(t) = \frac{1}{N} \sum_i \langle x_i(t) x_i(0) \rangle_\xi$ . We also consider the population averaged autoresponse  $r(t) = \frac{1}{N} \sum_i \lim_{\epsilon \rightarrow 0} \frac{1}{\epsilon} \langle x_i^\epsilon(t) - x_i(t) \rangle_\xi$ , where  $x_i^\epsilon(t)$  is the neural activity if Eq. (1) is perturbed by a term  $\epsilon \delta(t)$  along direction  $i$ .

Standard linear response theory gives

$$r(t > 0) = \frac{1}{N} \sum_\alpha \exp(-k_\alpha t) \stackrel{N \rightarrow \infty}{\rightarrow} \int \mathcal{D}k \exp(-kt), \quad (8)$$

where in the last line we have taken the limit of the sum of eigenvalues to an integral over their probability density, with integration measure  $\mathcal{D}k \equiv p(k) dk$ , valid for large  $N$ . In this limit, using our random matrix theory (see



Section B), we find  $A(t)$  has the expression

$$A(t) = \frac{1 + \nu^2}{1 - \nu^2} \int \frac{\mathcal{D}k}{2k_x} \exp(-k|t|) - \frac{2\nu^2}{1 - \nu^2} \int \frac{\mathcal{D}k_1 \mathcal{D}k_2}{k_1 + k_2} \exp(-k_1|t|). \quad (9)$$

$r(t)$  depends only on the eigenvalue distribution, and not on the eigenvectors.  $A(t)$  instead also depends on the eigenvectors' distribution, as reflected by the parameter  $\nu$ . The first term in Eq. (9) is the only one present in the limit of a normal network  $\nu \rightarrow 0$ , while the second term reflects a non-vanishing overlap between eigenvectors in the non-normal case (see Section B).

Let us first focus on the equal-time variance  $A(0)$ . As for the archetypal choice of  $J$ , the variance can diverge as we approach criticality. It's divergent behavior near criticality is described by the exponent  $d$  characterizing the density of nearly critical modes

$$p(k_x) \stackrel{k_x \rightarrow 0}{\sim} k_x^{d-1} \quad (10)$$

Indeed, we can note that, when the variance diverges, the first term in Eq. (9) dominates, behaving like

$$\sim \int \frac{p(k_x) dk_x}{k_x + \delta} \sim \int \frac{k_x^{d-1} dk_x}{k_x + \delta} \propto \begin{cases} \delta^{d-1} & d < 1 \\ \text{const} & d > 1 \end{cases} \quad (11)$$

where we performed the integration over the dummy variable  $k_y$  and introduced the small distance  $\delta$  from criticality. An analogous expression to Eq. (11) can be found for the variance of classical critical phenomena [24–26]. There, the eigenmodes are the Fourier modes, with associated wave-vector  $\vec{k}$ . The density of nearly critical modes obeys  $p(\|\vec{k}\|) \sim \|\vec{k}\|^{d-1}$ , where  $d$  cannot be chosen arbitrarily as in here, but corresponds to the system's spatial dimension. In analogy, we call  $d$  the system's effective spatial dimension, which here can also take non discrete values. As in classical critical phenomena, there is a critical dimension  $d_c = 1$ , above which the variance remains finite, while for smaller  $d$  it diverges as we approach criticality  $\delta \rightarrow 0$ . In the nonlinear regime, the critical dimension typically discriminates between mean-field criticality ( $d > d_c$ ), and criticality that could be characterized by a non-Gaussian fixed point ( $d \leq d_c$ ), requiring a renormalization group analysis. We further discuss the potential implications of this analogy in Section IV. A divergence of the variance in the linear system occurs also with the archetypal Gaussian connectivity: a saturating transfer function is required to keep the variance finite. Note that our ensemble instead provides connectivity choices that remain well-defined at the critical point, even in the linear case. A difference between the archetypal Gaussian connectivity and the one from our ensemble with matching eigenvalue distribution (i.e. uniform on the ellipse), is that the latter has dimensionality  $d = 1.5$ , so the system has finite variance.

We now focus on the asymptotic long-time dependence of  $r(t)$  and  $A(t)$ . As for  $A(0)$ , this is naturally characterized by the marginal distribution  $p(k_x)$  of decay constants of nearly critical modes, through the exponent  $d$ . In addition, the conditional distribution of oscillation frequencies  $p(k_y|k_x)$  for a given decay constant is now important. We find this quantity to control whether the decay in time is power-law or exponential. Differently than for  $A(0)$ , a characterization for a generic  $p(k_y|k_x)$  is hard in this case. To enlighten the role of oscillation frequencies, we consider the case of  $p(k_y|k_x)$  uniform, that is an eigenvalue distribution of the form

$$p(k) \stackrel{k_x \rightarrow 0}{\sim} k_x^a \theta(Ak_x^b - |k_y|), \quad (12)$$

with  $A, b > 0$ . As illustrated in Fig. 3(a), two exponents characterize the distribution. Exponent  $b$  characterizes the maximum oscillation frequency of nearly critical modes  $|k_y|_{max} \propto k_x^b$ , i.e. the boundary of the eigenvalue distribution. Exponent  $a$  characterizes the density of nearly critical modes Eq. (10) through  $d = a + b + 1$ . These exponents also characterize the dynamics in a very direct way. As illustrated in Fig. 3(b) and (c), we find that, for slow enough oscillations of nearly critical modes,  $b \geq 1$ , the dynamics follow a power-law decay in time, with exponents  $r(t) \sim t^{-d}$  and  $A(t) \sim t^{-(d-1)}$ . Instead, when oscillations are too fast,  $b < 1$ , the decay is slower, potentially exponential and oscillating.

Considering  $r(t)$  as an example, this can be easily seen by integrating Eq. (8) over  $k_y$  and passing to the dimensionless variable  $p \equiv k_x t$ , obtaining

$$r(t) \stackrel{t \rightarrow \infty}{\sim} \frac{1}{t^{a+2}} \int_0^\infty dp p^a \exp(-p) \sin(p^b t^{1-b}) \quad (13)$$

We can see that, if  $b > 1$ , oscillations are unimportant in the long-time limit, as we can expand the oscillating term  $\sin(x) \sim x$  in the integrand, recovering the power-law scaling  $r(t) \sim t^{-d}$ . If  $b < 1$ , instead, oscillations interfere with the build up of nearly critical modes into a pure power law.

The reasoning is completely analogous for  $A(t)$ , noting that the first term in Eq. (9) dominates in the long-time limit. This means that, though the degree  $\nu$  of non-normality of the network affects quantitatively  $A(t)$ , it does not affect its power-law decay exponent. This is illustrated in Fig. S1.

Note that in the archetypal case of a Gaussian connectivity, the decay of both  $r(t)$  and  $A(t)$  is known to be exponential. The emergence of power-laws is a novelty of certain connectivities here considered, whose nearly critical modes have sufficiently slow oscillation frequencies ( $b > 1$ ). This is of relevance for the ubiquitous observation of power-laws in neural dynamics. For example, as discussed in Section IV, a power-law behavior in the response function could be relevant for the phenomenon of neural avalanches [11–13].

Finally we comment on parameter  $A$  appearing in Eq. (12). This can stretch the distribution along the

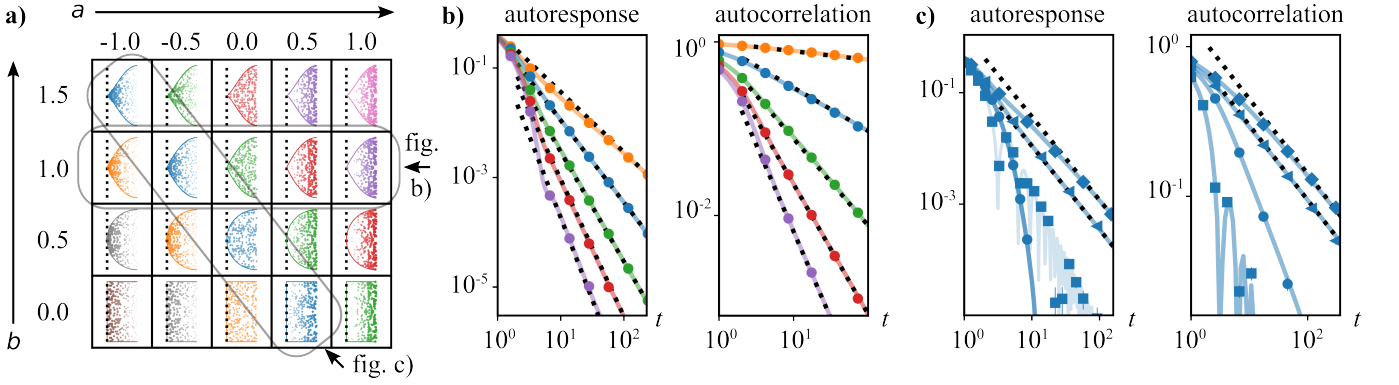


Figure 3. (a) Eigenvalue distributions. Grid showing different distributions of nearly critical eigenvalues for varying  $a$  and  $b$ . Distributions with the same  $d = a + b + 1$  share the same color (diagonals). Within each  $k_x$ - $k_y$  plane (i.e. each square), the dashed vertical line represents the critical line of instability at  $k = 0$ . (b) Power-law decay, controlled by  $d$ . The autoresponse  $r(t)$  and normalized autocorrelation  $A(t)/A(0)$  are shown for fixed  $b = 1$  and varying  $d$  (equivalently  $a$ ), corresponding to the  $(b = 1)$ -row in (a) and colored accordingly. Solid curves: theory; markers: simulations; dashed, black lines: power-law decay with exponent  $d$  for the autoresponse and  $d - 1$  for the autocorrelation. For the autocorrelation, rather than the case  $d = 1$  (orange), the case  $d = 1.1$  is shown, to avoid long simulation times. (c) Transition from power-law to faster decay, controlled by  $b$ . The autoresponse and normalized autocorrelation are shown for fixed  $d = 1.5$  and varying  $b = 1.5$  (diamonds),  $1$  (triangles),  $0.5$  (circles),  $0$  (squares), corresponding to the blue diagonal in (a). Solid curves: theory; markers: simulation. For  $b \geq 1$ , we see a power law decay with exponent  $d$  (dashed, black lines). For  $b < 1$  the decay is faster. Other parameters:  $N = 10^2$ ,  $\nu = 1/\sqrt{3}$ ,  $A = 1$ .

imaginary axis. As we see from Eq. (7), this controls the degree of symmetry  $\tau$  of the connectivity matrix. We note parameter  $A$ , therefore symmetry, does not affect the power-law decay exponent, though it affects quantitatively the shape of  $A(t)$  and  $r(t)$ . This is illustrated in Fig. S1.

We conclude remarking that the power-law scaling found in this section, but also in the following sections, only depend on a very generic property of the eigenvalue distribution, namely the scaling Eq. (10). As we have seen, the shape of the boundary of the distribution, here controlled by  $b$ , or its stretching, controlled by  $A$ , do not affect the power-law exponents for a fixed  $d$ .

## B. Dimensionality

A common measure of neuronal activity is its covariance matrix. Here we consider the equal-time covariance  $C_{ij} = \langle x_i(t) x_j(t) \rangle$  and the long time-window covariance  $C_{ij} = \lim_{T \rightarrow \infty} \frac{1}{T} \langle \hat{x}_i(0) \hat{x}_j(0) \rangle$ , where we defined the Fourier transformed neural activity  $\hat{x}_i(\omega) = \int_{-\frac{T}{2}}^{\frac{T}{2}} dt e^{-i\omega t} x_i(t)$ . A common analysis of the covariance is by its principal components. Being a covariance matrix,  $C$  is positive semi-definite, so one can always consider its eigenmodes decomposition

$$C = \sum_{\alpha} U_{\alpha} c_{\alpha} U_{\alpha}^T \quad (14)$$

with the eigenvectors  $U_i$  identifying orthogonal directions of neuronal variability, and the eigenvalues  $c_i > 0$  its intensity along that direction. Recent research has shown

considerable interest for the dimensionality of neuronal activity [17, 27, 28], which is an estimate of how many of the strongest principal components are required to explain most of neuronal variability. Various experimental studies have found low dimensional activity in the brain [15–17], and sufficiently low dimensionality is argued to be necessary for optimal stimulus encoding [17]. A common measure of dimensionality is the participation ratio [9, 29]

$$D \equiv \frac{(\sum_{\alpha} c_{\alpha})^2}{\sum_{\alpha} c_{\alpha}^2} = \frac{(\text{Tr}[C])^2}{\text{Tr}[C^2]} \quad (15)$$

which can conveniently be reduced to traces of powers of the covariance matrix. The latter we are able to compute with our random matrix theory. We now proceed to characterize the behavior of dimensionality near criticality.

### 1. Equal time covariance

Let us start considering the equal-time covariance. Once again, we find that dimensionality is controlled by the density of nearly critical modes Eq. (10) through the exponent  $d$ .

Note the numerator in Eq. (15) corresponds to  $A(t=0)^2$  given in Eq. (9). We already discussed its diverging behavior near criticality in Eq. (11). The expression for the denominator  $\text{Tr}[C^2]$  is lengthy and we do not report it here. The expression is analogous to Eq. (9), containing a first term surviving for  $\nu \rightarrow 0$ , which is the one dominating the divergent behavior near criticality  $\delta \rightarrow 0$ , in addition to terms due to the network

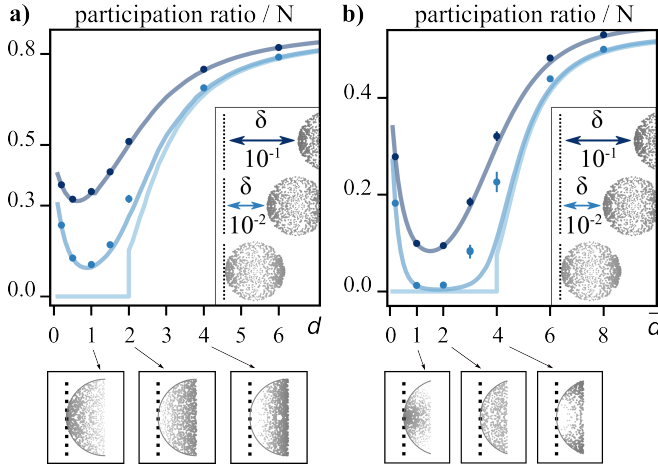


Figure 4. Transition from high to low dimensionality. The participation ratio is shown for the equal-time (a) and long time-window (b) covariance, as a function of  $d$  or  $\bar{d}$ , respectively. Curves in lighter blue correspond to decreasing values of  $\delta$  (see inset). Solid curves: theory; markers: simulation. Only theory is shown for  $\delta = 0$  (lightest blue), at which the transition is infinitely sharp. Note an eventual offset between theory and simulation for the smaller  $\delta$  is due to finite size effects. At the bottom, distributions of nearly critical eigenvalues are shown for some example values of  $d$  and  $\bar{d}$ . Other parameters: (a)  $N = 10^3$ ,  $\nu = 1/\sqrt{3}$ ,  $b = 0.5$ ,  $A = 1$ ; (b)  $N = 8 \cdot 10^3$ .

non-normality, analogous to the second term in Eq. (9). The dominating divergent term behaves as

$$\sim \int \frac{p(k_x) dk_x}{(k_x + \delta)^2} \sim \int \frac{k_x^{d-1} dk_x}{(k_x + \delta)^2} \propto \begin{cases} \delta^{d-2} & d < 2 \\ \text{const} & d > 2 \end{cases} \quad (16)$$

Combining Eq. (11) and Eq. (16) into Eq. (15), we therefore distinguish the behavior of dimensionality into three regions: for  $d > 2$ , dimensionality is constant even at criticality; for  $1 < d < 2$  we observe low-dimensional activity, decaying as  $\delta^{2-d}$ ; for  $d < 1$  again we have low-dimensional activity, but decaying as  $\delta^d$ . As can be seen in Fig. 4(a), we therefore have a transition from high to low dimensional activity at  $d = 2$ . The transition becomes infinitely sharp at criticality. Close to criticality, dimensionality will show an optimum for connectivities with dimension  $d = 1$ , at which the dimensionality of the input noise is reduced the most.

Once again, we show in Fig. S1 that the detailed shape of the eigenvalue distribution does not affect the presence of a transition from high to low dimensional activity. In fact, for  $d < 2$ , eigenvalue distributions with different boundaries and stretchings even collapse to the same curve.

As for the previous section, we also show in Fig. S1 that, while the degree of non-normality has a quantitative effect on dimensionality, it does not affect the power-law scaling described here, and thus the presence of a transition from low to high dimensional activity at  $d = 2$ , with an optimum at  $d \sim 1$ .

## 2. Long time-window covariance

For the long-time window covariance the reasoning is completely analogous. Integrals of the same kind as Eq. (11) appear (see Section B). The main difference is that in Eq. (11), the relevant direction of integration approaching the critical point  $k = 0$ , is the one along the real axis,  $k_x$ . For the long-time window covariance, the relevant direction is the radial one,  $\rho$ , where we defined  $k \equiv \rho e^{i\phi}$ . We therefore introduce a radial dimension  $\bar{d}$  controlling the density of nearly critical modes along the radial direction

$$p(\rho) \stackrel{\rho \rightarrow 0}{\sim} \rho^{\bar{d}-1} \quad (17)$$

The results are then completely analogous to those for the equal-time covariance, and are shown in Fig. 4(b). For  $\bar{d} > 4$ , dimensionality is constant even at criticality; for  $2 < \bar{d} < 4$  we observe low-dimensional activity, decaying as  $\delta^{4-\bar{d}}$ ; for  $\bar{d} < 2$  again we have low-dimensional activity, but decaying as  $\delta^{\bar{d}}$ . Close to criticality, dimensionality will show an optimum for connectivities with dimension  $\bar{d} = 2$ , at which the dimensionality of the input noise is reduced the most. Note that in the archetypal case of Gaussian  $J$ , the decay of dimensionality is known to behave like  $\delta^2$ . This is reproduced also for our matrix with matching distribution of eigenvalues (i.e. uniform on the circle). Indeed, such distribution has radial dimension  $\bar{d} = 2$ . Interestingly  $\bar{d} = 2$  is also where we have an optimal reduction of the dimensionality of input noise. Note, however, that many shapes other than circular uniform can have  $\bar{d} = 2$ .

## C. Principal components spectrum

The participation ratio Eq. (15) is a quantity derived from the first two moments of the principal components eigenvalues  $c$ , appearing in Eq. (14). It is also interesting to study the full distribution  $p(c)$  of these eigenvalues. For example, a recent experimental study has considered the principal components of neural activity in V1 of mice, during the encoding of image stimuli Stringer et al. [17]. They plot the eigenvalues  $c$  against their rank, that is their discrete labeling when they are ordered from largest to smallest. They find a power-law decay with exponent  $\alpha = 1$ , which they theoretically argue to be optimal for encoding visual stimuli: larger  $\alpha$  would correspond to fewer details encoded, while a smaller  $\alpha$  would be too sensitive to details and correspond to a fractal representation. Recent theoretical work has derived a similar power-law decay for a network governed by Eq. (1), for the archetypal choice of  $J$  Hu and Sompolinsky [9]. They find a power-law exponent of  $\alpha = 1.5$ , different from the one experimentally observed. It is interesting, therefore, to see whether different configurations of synaptic strengths can vary the power-law exponent, eventually tuning it to the optimal value.

Deriving an expression for  $p(c)$  for any value of the degree of non-normality  $\nu$  is a hard task that we leave for future work. However, we can easily derive  $p(c)$  for the normal case  $\nu = 0$ , and study numerically what happens for  $\nu \neq 0$ .

Let us first consider the principal components of the time integrated covariance. For  $\nu = 0$ , the principal components eigenvalues  $c$  are simply related to the connectivity eigenvalues  $k = \rho e^{i\phi}$  by  $c = \rho^{-2}$  (see Section B). Therefore,  $p(c) = p(\rho(c)) c^{-\frac{3}{2}}$ . Once again, we see that a power-law emerges, that is controlled by the density of nearly critical modes Eq. (17):  $p(c) \stackrel{c \rightarrow \infty}{\sim} c^{-\frac{d+2}{2}}$ . It follows that the power-law decay of  $c$  with its rank  $n$  is  $c \sim n^{-\alpha}$ , with  $\alpha = 2/\bar{d}$ . Therefore, as illustrated in Fig. 5(a), varying the connectivity's density of nearly critical modes tunes the power-law decay of the principal components spectrum. Numerically, we find that also the degree of non-normality  $\nu$  controls the decay exponent. As illustrated in Fig. 5(b), for a fixed  $\bar{d}$ , increasing  $\nu$  increases the exponent  $\alpha$ . This effect is weak for small or intermediate values of  $\nu$ , and starts becoming apparent for large values of  $\nu$ . Finally, let us note that a uniform elliptical eigenvalue distribution corresponds to  $\bar{d} = 2$  and therefore to  $\alpha = 1$  in our ensemble. This is different from the value  $\alpha = 1.5$  found for the archetypal  $J$ , which has the same eigenvalue distribution. The difference is caused by the different statistics for the eigenvectors, which in the archetypal case are strongly correlated to the eigenvalues. Interestingly, the exponent  $\alpha = 1.5$  is approached in our case by increasing  $\nu$  to a strong degree of non-normality  $\nu \sim 0.85$ . As we comment in IIIB, strong non-orthogonality is indeed a feature of the eigenvectors corresponding to the archetypal  $J$ .

As illustrated in Fig. 5(c-d), completely analogous results follow for the equal-time covariance. The only difference is that here  $c = k_x^{-1}$  (see Section B), thus the power-law exponent  $\alpha$  is still controlled by the density of nearly critical modes Eq. (10), but the one obtained approaching the critical point along the real axis. Specifically, we have a power-law decay with rank  $c \sim n^{-\alpha}$ , with  $\alpha = 1/d$ .

### III. CONNECTIVITY STATISTICS

In this section, we present further insights into the statistics of the connectivity matrices of our ensemble, both in synaptic and in dynamics space.

#### A. Leading order synaptic statistics

First, let us comment on the leading order synaptic statistics, Eq. (6) and Eq. (7). These depend on both the degree of non-normality  $\nu$  and the second moments of the eigenvalue distribution.

Let us first fix  $\nu$  and look at the effect of the eigenvalue distribution. Notice the synaptic gain  $g$  is con-

trolled by the overall spread of eigenvalues on the complex plane. Unsurprisingly, increasing the spectral radius of the eigenvalue distribution corresponds to proportionally increasing the synaptic gain. The degree of symmetry  $\tau$  is instead controlled by the relative spread of the distribution along the real and imaginary axes. Notice that Eq. (7) generalizes to any eigenvalue distribution in our ensemble, a fact that could already be observed for the elliptical distribution corresponding to the archetypal  $J$ : there, varying  $\tau$  corresponds to stretching the ellipse along the imaginary or real axis (see e.g. Fig. 1). In fact, choosing  $\nu^2 = \frac{1-\tau^2}{3+\tau^2}$ , we exactly reproduce the synaptic statistics of the archetypal approach: for a given  $g$  and  $\tau$ , the archetypal approach produces a certain uniform elliptical eigenvalue distribution; initializing a matrix in our ensemble with such eigenvalue distribution, Equations (6) and (7) give back exactly the same values of  $g$  and  $\tau$  (see Fig. 6(a) for an example). For the special case  $\tau = 0$ , we have  $\nu = 1/\sqrt{3} \sim 0.577$ . Note, however, that the connectivity in the two ensembles are still different: in our ensemble, synaptic strength statistics have a more complicated subleading order structure while, specularly, the archetypal connectivity presents strongly fine-tuned correlations between eigenvalues and eigenvectors. We further elaborate on these differences later in this section.

For a fixed eigenvalue distribution, notice  $g$  and  $\tau$  can still be partially tuned by the degree of non-normality  $\nu$ . For example, stronger normality of the network (i.e. smaller  $\nu$ ) corresponds to stronger (anti)symmetry. Note that, as should be expected, perfect (anti)symmetry is only achieved in the limit of a normal network  $\nu = 0$  and an eigenvalue distribution collapsed on the (imaginary) real axis. Regarding the effect of  $\nu$  on the synaptic gain  $g$ , notice a too strong non-normality  $\nu \rightarrow 1$  makes the synaptic gain diverge. However, also note that  $g$  remains of  $\mathcal{O}(1)$  for considerably strong  $\nu \sim 0.9$  (Fig. 6(a)). More extreme degrees of non-normality require correlations between eigenvalues and eigenvectors, to keep  $g$  order unity. We discuss this case in the following subsection.

#### B. Strongly non-normal regime

We can further elucidate the meaning of the non-normality parameter  $\nu$  by looking into the connectivity eigenvectors. This also allows us to better understand the differences between our ensemble and the archetypal one. It is instructive to look at a naive approach in defining the eigenvector statistics. As we stated in Section I, we want to be agnostic regarding the direction taken by the random eigenvectors in neuronal space. The simplest - but too naive - way of implementing this would be to initialize  $V = G$  as random Gaussians, rather than  $V = O + \nu G$  as in Eq. (5). The problem is that eigenvectors defined in this way take on too random directions, having too strong overlaps. This causes the synaptic gain  $g$  to take on arbitrarily large values, when it should instead be of

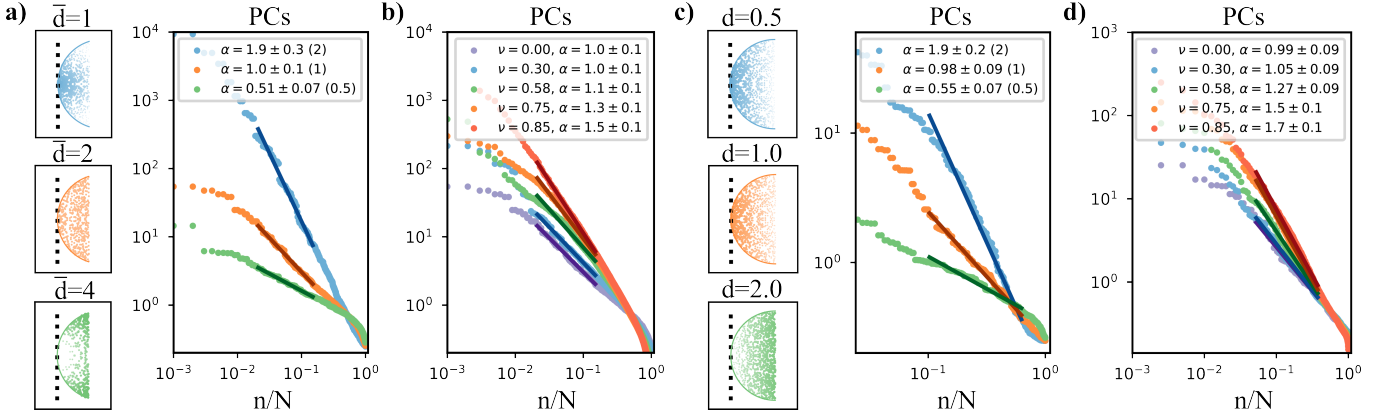


Figure 5. Connectivity controls the principal components spectrum. Covariance eigenvalues plotted against their fractional rank  $n/N$ . (a-b) Case of the long time-window covariance. (c-d) Same as (a-b), but for the case of the equal-time covariance. (a) Case  $\nu = 0$ . Shown for connectivities having eigenvalue distributions with varying  $\bar{d}$  (shown on the left and colored accordingly). Markers: simulation; lines: fitting power-law; legend: mean and standard deviation of the power law exponent  $\alpha$ , found for 48 independent realizations of the connectivity. Theoretical prediction in parenthesis. (b) Same as (a), but for fixed  $\bar{d} = 2$  and varying  $\nu$  (see legend). Other parameters: (a-b)  $N = 10^3$ ,  $\delta = 0.01$ ,  $b = 0.5$ ,  $A = 1$ ; (c-d)  $N = 4 \cdot 10^2$ ,  $\delta = 0.01$ .

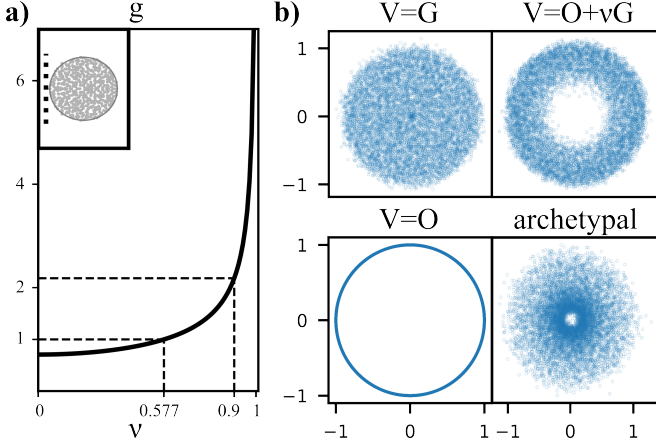


Figure 6. (a) Synaptic gain  $g$  as a function of the degree of non-normality  $\nu$ , for the case of a uniform circular distribution (inset), as that found in the archetypal connectivity for  $g = 1$  and  $\tau = 0$ . The dotted lines highlight the special value  $\nu = 1/\sqrt{3} \sim 0.577$ , for which  $g = 1$  is recollected. Also the value  $\nu = 0.9$  is highlighted, for which  $g$  is still of  $\mathcal{O}(1)$ . (b) Eigenvalues of the normalized eigenvectors' matrix  $V$ , for different choices of  $V$ . For the case  $V = O + \nu G$ ,  $\nu = 0.8$ .  $N = 10^2$  and we show eigenvalues from  $10^2$  independent realizations of the eigenvectors.

order unity to have physical meaning. This can be visualized by looking at the eigenvalues of  $V$  (Fig. 6(b)). For  $V = G$ , these are uniformly distributed in a circle, and can get arbitrarily close to zero. This means  $V^{-1}$ , which also appears in the definition of the connectivity  $J$ , Eq. (3), can have arbitrarily large eigenvalues, and is thus unbounded, causing also  $g$  to be unbounded as a consequence. On the other hand, notice that in the trivial case of a normal network,  $V = O$ , the eigenvalues are exactly constrained to the unit circle, and the problem

does not occur. To have a well defined connectivity with  $g = \mathcal{O}(1)$ , we introduce non-orthogonality in the eigenvectors gradually, shifting away from the orthogonal case by increasing  $\nu$ , through the choice  $V = O + \nu G$ . Notice that in this case the eigenvalues of  $V$  cannot get arbitrarily close to zero, but are constrained to be outside of an inner circle, which will shrink back to zero as  $\nu \rightarrow 1$ . This is the same mechanism occurring for the eigenvectors of the archetypal connectivity. Notice that in this case the inner circle has a very small radius, which in our approach would correspond to values of  $\nu$  very close to 1 and a nonphysical synaptic gain  $g = \mathcal{O}(\sqrt{N})$ , diverging with the system size. In fact, such strong degree of non-normality in the archetypal  $J$  can only be achieved through a fine-tuned correlation between eigenvalues and eigenvectors, which ensures that all diverging contributions in Eq. (3) are tightly balanced.

Our theoretical predictions do not include this regime of extreme non-normality. Nevertheless, we are able to extend our method of initializing a connectivity with arbitrary eigenvalue distribution also to this regime, so to study it numerically. Details on the method are found in A3. The idea is to start from the archetypal  $J$  for  $\tau = 0$ , which naturally implements the strongly non-normal eigenvectors and their correlations with eigenvalues. It's eigenvalue distribution will be uniform on the circle. We can obtain other eigenvalue distributions by continuously shifting the eigenvalues into some new position in the complex plane, such that they are distributed according to the new desired distribution. The intuition is that the continuous shift preserves to some extent the tight correlations between eigenvalues and eigenvectors, such that the connectivity remains well defined even if the eigenvectors are strongly non-orthogonal. We verify numerically that indeed this method ensures a well defined  $g = \mathcal{O}(1)$ . Our numerical simulations show a be-

havior analogous to that found in the previous section, when the eigenvalue distribution is varied. As shown in Fig. 7(a-b), dimensionality as a function of the density of nearly critical modes, as parameterized by  $d$  or  $\bar{d}$ , presents a similar shape as that shown in Fig. 4. In particular, an optimum is present at which the dimensionality of the input noise is most reduced. As can be seen in Fig. 7(c-d),  $d$  or  $\bar{d}$  also control the power-law decay exponent of the principal components spectrum. For the autoresponse function, the results are identical to those found in the previous section, as this function does not depend on the eigenvector statistics. The only evidently different behavior is shown by the autocorrelation function. There, we find the strong non-orthogonality of the eigenvectors has a dominating effect of enforcing an exponential decay and a divergence of the neuronal variance  $A(0)$ , independently of the eigenvalue distribution. It is unclear which degree of non-normality in the connectivity would be preferred by brain networks. Future work may explore the computational benefits of the different regimes, or devise methods to extract the information on non-normality from experimental data.

### C. Subleading order synaptic statistics

As stated in Section I, we find that to leading order in the number of neurons, the synaptic statistics are Gaussian and given by Eq. (6) and Eq. (7). In particular, only second order reciprocal motifs are present. We can prove that all other second order motifs are absent and that higher order motifs appear with subleading order probability in the number of neurons. Specifically, writing the connectivity in dimensionless units  $\bar{J} := J\sqrt{\frac{N}{g}}$ , we prove that higher order cumulants  $\langle\langle\bar{J}_{i_1 i_2} \dots \bar{J}_{i_{2n-1} i_{2n}}\rangle\rangle$  are of order  $O\left(\frac{1}{\sqrt{N}}\right)$  for  $n = 3$  and of order  $O\left(\frac{1}{N}\right)$  for any other  $n > 3$ . We also prove that the only nonvanishing cumulants are those for which all indices  $i_1, \dots, i_{2n}$  are matched in pairs. For second order cumulants, this means only reciprocal motifs, associated with the cumulant  $\langle\langle J_{ij} J_{ji} \rangle\rangle$ , are present. For example, instead, cumulants like  $\langle\langle J_{ij} J_{kj} \rangle\rangle$ ,  $\langle\langle J_{ji} J_{jk} \rangle\rangle$  or  $\langle\langle J_{ij} J_{jk} \rangle\rangle$ , associated, respectively, with divergent, convergent, or chain motifs are null (see Fig. 1 for a schematic representation).

In actual experiments recording synaptic strengths, we only have one brain network to work with, so we do not measure the statistical averages  $\langle \rangle$  across different realizations of the connectivity, but empirical averages across all synapses within a single realization of the connectivity. For example we would not measure  $\langle\langle J_{ij} J_{ji} \rangle\rangle$ , but  $\frac{1}{N(N-1)} \sum_{i \neq j} J_{ij} J_{ji}$ . Note that the scaling with  $N$  of cumulants is such that the central limit theorem holds, so statistical averages are well estimated by the corresponding empirical averages, just like in the archetypal case of perfectly Gaussian  $J$ .

Though higher order cumulants are vanishingly small in  $N$ , collectively, they still have a macroscopic effect

in eigenmodes space. Indeed, these are the cumulants controlling the shape of the eigenvalue distribution and the eigenvectors' non-orthogonality  $\nu$ . This must be so, because a connectivity with statistics exactly truncated to the leading order, that is Eq. (6) and Eq. (7) only, corresponds to the archetypal connectivity, for which we know the eigenvalue distribution is fixed to be uniform elliptical. Our dynamics space approach to connectivity therefore shows how statistics that may appear to be irrelevant in synaptic space, because of their subleading order, have in fact a macroscopic effect in dynamics space. This effect can be macroscopically observed in the wide range of different behaviors showcased by the dynamical quantities discussed in Section II. A dynamics space approach in modeling the networks' connectivity is therefore important to capture this wide range of behaviors.

Note that the connectivity statistics has a somewhat specular behavior with respect to the archetypal approach. In the archetypal approach, imposing simple Gaussian statistics in synaptic space causes intricate correlation structures in eigenmodes space. Similarly, assuming relatively simple statistics in eigenmodes space, like the independence between eigenvalues and eigenvectors, corresponds to a complex cumulant structure in synaptic space. A difference, though, is that such structure is only of subleading order in  $N$ .

The fact that beyond Gaussian synaptic statistics are vanishingly small does not mean that the structure within the connectivity that controls the shape of the eigenvalue distribution consists of small fine-tunings. One needs to be careful to distinguish the statistics obtained by averaging over different connectivity realizations and the structure within a single realization. Within the single realization, the structure controlling the eigenmodes statistics does not rely on small fine-tunings. We test this by perturbing every synaptic strength  $J_{ij}$  with some independent Gaussian noise  $\delta J_{ij} \sim \mathcal{N}\left(0, \frac{\epsilon^2}{N}\right)$ , with  $\epsilon = 0.01, 0.1$ , corresponding to a perturbation of order 1% and 10% of the typical synaptic strength (see S2). We verify numerically that the dynamical behaviors shown in Section II are robust to these perturbations. A way to interpret our result on the non-Gaussian synaptic statistics being of subleading order is therefore the following: the synaptic structures controlling the dynamics are not detectable by measuring the abundance of generic connectivity motifs through the empirical averaging over synapses. These structures are less generic than motifs and therefore invisible to a motif analysis.

## IV. DISCUSSION

We have developed a dynamics space approach to model the connectivity of random networks. The method allows one to define connectivities with any desired



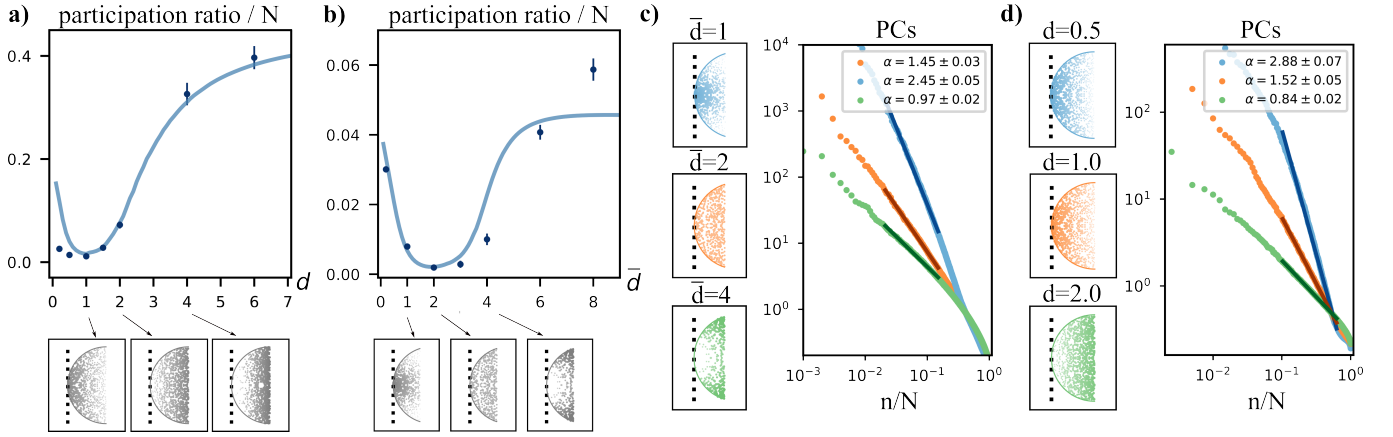


Figure 7. Strongly non-normal regime. (a-b) are analogous to Fig. 4(a-b), while (c-d) are analogous to Fig. 5(a) and Fig. 5(c). The same eigenvalue distributions are considered, but with strongly non-orthogonal eigenvectors. (a-b) participation ratio of the equal-time (a) and long time-window (b) covariance.  $\delta = 0.01$ . Markers: simulation. Solid line: theory for  $\nu = 0.8$  (a) and  $\nu = 0.9$  (b), i.e. *not* in the strongly non-normal regime, is shown for comparison. (c-d) Principal components spectrum for the long time-window (c) and equal-time (d) covariance.

shape of the eigenvalue distribution and degree of non-normality. This greatly expands the ensemble of available connectivity matrices and reveals a wide range of previously unexplored network behaviors.

The more traditional synaptic space approach can justify the choice of connectivity statistics based on experimental data on synaptic strengths and motifs [10]. But a large, if not prevalent, part of experiments on brain networks focuses on parallel recordings of neuronal dynamics. Our dynamics space approach represents a fundamental theoretical step in modeling a network's connectivity based on this wealth of experimental data: We have shown how the distribution of the connectivity's eigenmodes has a direct effect on the network dynamics. This effect is quantifiable in terms of scaling laws and power-law exponents, which are quantities readily testable on experimental data and are in fact ubiquitously observed in brain networks [13, 14, 17]. Future work will explore network models whose connectivity choice is informed by such experiments, and may explain their results. Below we report some experimental works that could be intriguingly related to our findings.

A novel finding of our work is the emergence of a power-law decay in time of correlation and response functions, for certain distributions of oscillation frequencies of the network eigenmodes. A power-law behavior of the response function is relevant for the phenomenon of neural avalanches. Avalanche properties are linked to the system's response to a perturbation, as it relaxes into a quiescent state [30]. Power-laws are typically observed for neural avalanches [11, 12] and recent work has observed variability in their exponents [13]. Our theory may be used to explain such variability, as it provides a mechanism by which connectivity can control the exponent governing the response's power-law decay.

In general, we show that all dynamical quantities studied in Section II can assume a wide range of power-law

exponents, controlled by the network's connectivity. This allows asking optimization questions: why would a network choose to learn a certain connectivity, with its specific dynamical behavior? How is that behavior optimal for computation? Note, for example, that a connectivity characterized by effective spatial dimension  $d \sim 1^+$  intriguingly optimizes multiple dynamical properties: The response, which relates to the system's memory of an input signal, has the slowest possible decay  $\sim t^{-d}$ , while simultaneously noise remains finite (recall the autocorrelation  $\sim t^{1-d}$  and the equal time variance  $\sim \delta^{d-1}$ ); at the same time, the dimensionality of input noise is optimally reduced, as shown by a minimum in the participation ratio.

Of particular interest for the question of optimization is the network's ability to tune the decay of its principal component spectrum with rank. Indeed, theoretical considerations suggest a decay exponent  $\alpha = 1$  for optimal image encoding, which is also experimentally found in V1 of mice [17]. Previous theoretical work has found an exponent  $\alpha = 1.5$ , for the archetypal connectivity [9]. Here we have shown how this exponent can be tuned into the optimal one by a different connectivity choice. In both our and previous work, only a white noise input is considered. Future work may study the more relevant case of a structured input, like natural images.

Recent works have shown that the large-scale statistics of neuronal recordings seem to approach a non-Gaussian fixed point [14, 31]. It would be interesting to study Eq. (1) in the nonlinear regime, applying the nonequilibrium renormalization group [25, 26] to look for the presence of a non-Gaussian fixed point. Note that in the case of the archetypal connectivity, mean-field theory applies and the large scale description of the network is in fact Gaussian [4, 32]. However, we have here noticed an analogy with classical critical phenomena, which suggests that for connectivities with a dimension  $d \leq d_c = 1$ ,

mean-field theory could break down and a non-Gaussian fixed point could emerge. The renormalization group methods are most naturally applied in the space of eigenmodes, which for classical critical phenomena are the Fourier modes [24]. Our definition of connectivity in eigenmode space may allow for a more natural transfer of the renormalization group methods to disordered networks. Recent work has applied these methods to a structured neural network and could be used as guidance [33].

Our work exposes how a purely synaptic space approach to connectivity may miss important dynamical consequences. We indeed show that a motif analysis cannot distinguish between connectivities with very different eigenmodes statistics, thus associated to different dynamical behaviors.

In the here proposed random matrix ensemble, we introduce the possibility to control the degree of non-normality of the network, and study its dynamical consequences. Our theoretical understanding also provides novel intuitions as to why, in the strongly non-normal regime, a fine-tuned correlation structure between eigenvalues and eigenvectors is needed. This intuition allows us to devise a novel method to control the connectivity's eigenvalue distribution, even in this regime. For this special case, we only performed a numerical study of the network dynamics. Building on our methods and insights, future work could develop an analytical theory for the strongly non-normal regime. For the connectivity eigenvalues, we identified a clear link with observable dynamical quantities in their power-law exponents. Instead, it is not yet clear to us which experimental quantity could help discriminate between different degrees of non-normality. Future work could help shedding light in this direction.

In this work, we only consider a fully connected network. Also, the connectivity does not implement Dale's law, which imposes neurons should be either purely excitatory or inhibitory. This is not problematic for effective models such as the one studied here. However, models that wish to capture a more microscopic description of biological neural circuits would find a limitation in our random matrix ensemble. It would be interesting to study how the eigenmode statistics should be defined, in order to reflect sparse connections and Dale's law in synaptic space. To this end, a work in the specular direction could be of inspiration [34], which derives the eigenvalue statistics that emerge from imposing the aforementioned conditions in synaptic space.

## ACKNOWLEDGMENTS

This work was partially supported by the Helmholtz Association, the Initiative and Networking Fund under project number SO-092 (Advanced Computing Architectures, ACA), and the German Federal Ministry for Education and Research (BMBF Grant 01IS19077A).

## Appendix A: Connectivity statistics

### 1. Details on the definition of the eigenmode statistics

Let us give the remaining details for the definition of the eigenmode statistics, presented in Section I. For simplicity, let us consider  $N$  even. Generalizing to  $N$  odd is straightforward. The realness of the elements of  $J$  imposes the condition that for any complex  $\lambda_\alpha$  and  $V_\alpha$ , there is an eigenmode index  $\alpha^*$  such that  $\lambda_{\alpha^*} = \lambda_\alpha^*$  and  $V_{\alpha^*} = V_\alpha^*$ . Note that since eigenmodes are randomly drawn in our ensemble, the probability that an eigenmode is real has null measure. Therefore we can assume all eigenmodes to be complex. By the constraint of real-valued  $J$  we only have  $N/2$  eigenmodes that are independent. We assign these eigenmodes to the first  $\alpha = 1, \dots, N/2$  of the eigenmode indices. The corresponding complex conjugate eigenmodes are assigned the index  $\alpha^* = \alpha + N/2$ . The first  $N/2$  eigenvalues are drawn independently according to the desired distribution  $p(\lambda)$ . The remaining half is obtained by complex conjugation.

The matrix of eigenvectors  $V$  is a linear combination of  $O$  and  $G$ . The scheme by which these two matrices are defined is the same. Let us consider, for example,  $G$ . Only the first  $\alpha = 1, \dots, N/2$  vectors  $G_\alpha$  are independent, and each has a real and an imaginary component. So we need to draw  $\frac{N}{2}2N = N^2$  random variables. We draw a real matrix  $g$  whose entries  $g_{\alpha i} \sim \mathcal{N}(0, 1/N)$  are independent, normally distributed variables. The first  $\alpha = 1, \dots, N/2$  vectors  $G_\alpha$  are then defined as

$$G_\alpha = \frac{1}{\sqrt{2}}g_\alpha + \frac{i}{\sqrt{2}}g_{\alpha+N/2}$$

In words, the first  $\alpha = 1, \dots, N/2$  rows of  $g$  constitute the real part of the vectors  $G_\alpha$ , the remaining rows  $\alpha + N/2$  constitute the imaginary part. The remaining vectors  $G_{\alpha^*}$  are obtained through complex conjugation.

The matrix  $O$  is defined in the same way, substituting  $G \rightarrow O$  and  $g \rightarrow o$ . The only difference is that  $o$  is a real orthonormal matrix, drawn from the Haar distribution. One can easily check that  $O$  satisfies the complex orthonormality relation  $OO^\dagger = \mathbb{I}$ .

Let us note that here we considered eigenvalue distributions for which the mean  $\langle \lambda \rangle = 0$ . A non-vanishing mean is trivial, as it amounts to sending  $J \rightarrow J + \langle \lambda \rangle \mathbb{I}$ , which can be reabsorbed in the definition of the leak term  $-x \rightarrow -(1 - \langle \lambda \rangle)x$  in Eq. (1).

### 2. Eigenvalue distributions used in simulations

Here we report the precise eigenvalue distributions used for the simulation of the dynamical quantities considered in Section II. Note that only the shape of the distribution near criticality is important in determining the scaling properties of dynamical quantities. Such

shape has been already reported in the main text and figures. The choice of the distribution for eigenvalues further away from criticality is arbitrary and irrelevant. We report it below for completeness.

For all quantities controlled by the exponent  $d$ , that is the density of nearly critical modes along the real axis, we used the following eigenvalue distribution

$$p(\mathbf{k}) = k_x^a \theta \left( A \left( 1 - (1 - k_x)^2 \right)^b - |k_y| \right) \quad \forall k_x \leq 1, \quad (\text{A1})$$

with  $\theta$  being the Heaviside function. The remaining half of the eigenvalues, with  $1 < k_x < 2$  and thus further away from criticality, are drawn in a specular manner: we send  $k \rightarrow 2 - k$ , draw the new variable according to Eq. (A1), and transform back to the original variable (see for example the distributions shown in Fig. 2). The choice of drawing eigenvalues in a specular manner is done for technical convenience, because then  $\langle \lambda \rangle = 0$  and there is no need to rescale the leak term in Eq. (1) (see A1). As stated above, also the precise shape of the distribution of the first half of the eigenvalues, Eq. (A1), is irrelevant. Only its limiting behavior for  $k_x \rightarrow 0$  is important, which follows Eq. (12), discussed in II A. The specific shape of the distribution has been chosen because for  $a = 0$  and  $b = 0.5$  it corresponds to a uniform elliptical distribution, as that of the archetypal  $J$ .

For all quantities controlled by the exponent  $\bar{d}$ , that is the density of nearly critical modes along the radial direction, we used the following eigenvalue distribution

$$p(\rho, \phi) = \rho^{\bar{d}-1} \theta \left( \arccos \left( \frac{\rho}{2} \right) - |\phi| \right) \quad \forall \rho \leq 1 \quad (\text{A2})$$

where  $k \equiv \rho e^{i\phi}$ . Note the expression in the Heaviside function constrains eigenvalues to lie within a circle. We fixed this shape for convenience, because for  $\bar{d} = 2$  it reduces to the uniform distribution on the circle, as that of the archetypal  $J$ . Again, the exact shape of the distribution away from criticality is irrelevant and we report it here for completeness. The remaining eigenvalues in the first half of the circle, i.e. with  $1 < \rho < \sqrt{2}$ , are drawn according to Eq. (A2), but are rejected and redrawn if they fall out of the semicircle, that is if  $k_x > 1$ . The remaining half of the eigenvalues are drawn specularly, as discussed in the paragraph above.

### 3. Strongly non-normal regime

Here we report details on the method presented in II B, to numerically implement connectivities in the strongly non-normal regime that have a desired shape of the eigenvalue distribution. The method produces the distributions presented in A 2.

We start initializing the archetypal Gaussian  $J$ , with  $g = 1$  and  $\tau = 0$ . Its eigenvalues  $\lambda_\alpha$  and associated right and left eigenvectors  $V_\alpha$  and  $V_\alpha^{-1}$  are derived numerically. The eigenvalues  $\lambda$  are uniformly distributed

on a circle of unit radius. We start from this distribution and continuously shift the eigenvalues into some new position, so that they follow a new desired distribution. The continuous shift of the eigenvalues preserves to some extent the correlation structure between eigenvalues and eigenvectors, which in the strongly non-normal regime is necessary to have a synaptic gain  $g = \mathcal{O}(1)$ .

We first focus on producing the eigenvalue distribution Eq. (A1). This distribution is characterized by the parameters  $A$ ,  $b$  and  $d$  (or equivalently  $a$ ). The starting uniform circular distribution has parameters  $A_0 = 1$ ,  $b_0 = 0.5$  and  $d_0 = 1.5$ . Consider  $k = 1 - \lambda$ . To produce the eigenvalue distribution Eq. (A1) we shift the eigenvalues  $k \rightarrow \bar{k}$  through the transformation

$$\bar{k}_x = k_x^{\frac{d_0}{d}} \quad (\text{A3})$$

$$\bar{k}_y = k_y \frac{B(\bar{k}_x; A, b)}{B(k_x; A_0, b_0)} \quad (\text{A4})$$

where we defined the distribution's boundary function

$$B(k_x; A, b) \equiv A \left( 1 - (1 - k_x)^2 \right)^b.$$

This transformation is applied to all eigenvalues with  $k_x \leq 1$ . The remaining half of the eigenvalues, with  $1 < k_x < 2$ , are transformed in the specular manner described in A 2. Intuitively, Eq. (A3) readjusts the eigenvalues closer or further to the critical point according to the new  $d$ . Eq. (A4) rescales the imaginary part so that it fits the new boundary of the distribution.

To obtain the distribution Eq. (A2) we use an analogous method, only that the transformation is performed on the polar coordinates of  $k = \rho e^{i\phi}$ . The target distribution is characterized by the parameter  $\bar{d}$ , and the original distribution has a parameter  $\bar{d}_0 = 2$ . We apply the transformation

$$\bar{\rho} = \rho^{\frac{\bar{d}_0}{\bar{d}}} \\ \bar{\phi} = \phi \frac{B(\bar{\rho})}{B(\rho)}$$

with boundary function

$$B(\rho) \equiv \arccos \left( \frac{\rho}{2} \right)$$

This transformation is applied to all eigenvalues with  $\rho \leq 1$ . As stated in A 2, the shape of the distribution for eigenvalues further from criticality is arbitrary and irrelevant. We give it here for completeness. The remaining eigenvalues with  $1 < \rho < \sqrt{2}$  which also are in the first semicircle  $k_x \leq 1$  are left untouched. The remaining eigenvalues in the second semicircle are transformed in the specular manner described in A 2.

### 4. Derivation of the synaptic statistics

We develop a method to compute moments (or cumulants) of the matrix elements of  $J$ . The calculations are

somewhat intricate and the precise details will be given elsewhere. Here we review the main ideas behind the calculation.

Looking at the definition Eq. (3), we can see that this involves being able to compute moments of the elements of the eigenvectors matrix  $V = O + \nu G$  and its inverse  $V^{-1}$  (commonly called the matrices of the right and left eigenvectors, respectively). For example, computing the second moment of  $J$  corresponds to

$$\langle J_{ij} J_{hk} \rangle = \sum_{\alpha\beta} \langle \lambda_\alpha \lambda_\beta \rangle_\lambda \left\langle V_{i\alpha} V_{\alpha j}^{-1} V_{h\beta} V_{\beta k}^{-1} \right\rangle_{O,G}$$

To proceed, we note that the inverse can be written as the infinite series

$$V^{-1} = \sum_{n=0}^{\infty} (-\nu)^n (O^\dagger G)^n O^\dagger,$$

where we used that  $O$  is unitary. Computing a certain moment of  $V$  and  $V^{-1}$  thus corresponds to computing an infinite number of moments of  $O$  and  $G$ . Being Gaussian, the moments of  $G$  can be computed using Wick's calculus [35], that is using the known result that moments of  $G$  factorize into the expectation of pairs of  $G$ , summing over all possible ways of pairing the  $G$ s. Similarly, moments of  $O$  can be computed using Weingarten's calculus [36–38], the analogous of Wick's calculus for orthogonal matrices. Weingarten's calculus is more complicated, but in the limit of large  $N$  it reduces to leading order to Wick's calculus [36].

There is still an infinite number of moments to compute and, at each order of  $\nu$ , a large number of terms arising from the combinatorics involved in Wick's calculus. At each order of  $\nu$ , however, only a few terms are of leading order in  $N$ . Using a Feynman-diagram representation [35], we are able to keep track of these leading order terms, which can be identified based on the topology of the associated diagrams. Once the terms of leading order in  $N$  are computed for any given order of  $\nu$ , we are able to resum all orders of  $\nu$  exactly. Note that therefore our results are exact in  $\nu$  and perturbative in  $N$ , which is naturally large.

With this method, we compute the second moments of  $J$ , Eq. (6) and Eq. (7). We do not compute explicitly higher order moments of  $J$ . Computing these would involve considering subleading order deviations of Weingarten's calculus from Wick's calculus. However, we are able to use the properties of the full Weingarten's calculus to prove the results presented in IIIC, like the fact that higher order moments of  $J$  are of subleading order in  $N$ .

## Appendix B: Derivation of dynamical quantities

Here we give details on the derivation of the dynamical quantities considered in Section II.

### 1. Autocorrelation and autoresponse

Let us start by considering the system's linear response matrix  $R(t)$ , which is the Green function of Eq. (1). In frequency domain this is defined as the solution to

$$(i\omega \mathbb{I} + \mathbb{I} - J)R(\omega) = \mathbb{I}, \quad (\text{B1})$$

which is

$$R(\omega) = (i\omega \mathbb{I} + \mathbb{I} - J)^{-1}. \quad (\text{B2})$$

Using the eigenmode decomposition of  $J$ , Eq. (3), we can rewrite Eq. (B2) as

$$R_{ij}(\omega) = \sum_{\alpha} \frac{1}{i\omega + k_{\alpha}} V_{i\alpha} V_{\alpha j}^{-1} \quad (\text{B3})$$

which in time domain reads

$$R_{ij}(t) = \sum_{\alpha} \exp(-k_{\alpha} t) V_{i\alpha} V_{\alpha j}^{-1} \quad (\text{B4})$$

The expression for the population averaged autoresponse Eq. (8), considered in IIA, directly follows from computing  $r(t) = \frac{1}{N} \sum_i R_{ii}(t)$ , noticing that  $\sum_i V_{i\alpha} V_{\alpha i}^{-1} = \delta_{\alpha,\alpha} = 1$ . The latter identity makes  $r(t)$  independent of the eigenvectors.

Let us now consider the time-lagged covariance matrix  $C_{ij}(t) \equiv \langle x_i(t) x_j(0) \rangle_{\xi}$ . This can be derived by plugging into its definition the formal solution  $x_i(t) = \int_{t'} \sum_j R_{ij}(t-t') \xi_j(t')$  and averaging over the noise. In frequency domain, the result is

$$C(\omega) = (i\omega \mathbb{I} + \mathbb{I} - J)^{-1} (i\omega \mathbb{I} + \mathbb{I} - J)^{-\dagger} \quad (\text{B5})$$

Using the eigenmode decomposition of  $J$ , Eq. (3), we can rewrite Eq. (B5) as

$$C_{ij}(\omega) = \sum_{\alpha\beta} G_{\alpha\beta}(\omega) V_{i\alpha} \left( \sum_h V_{\alpha h}^{-1} V_{\beta h}^{-1} \right) V_{j\beta} \\ G_{\alpha\beta}(\omega) \equiv \frac{1}{(\omega - ik_{\alpha})(\omega + ik_{\beta})} \quad (\text{B6})$$

which in time domain reads

$$C_{ij}(t) = \sum_{\alpha\beta} G_{\alpha\beta}(t) V_{i\alpha} \left( \sum_h V_{\alpha h}^{-1} V_{\beta h}^{-1} \right) V_{j\beta} \\ G_{\alpha\beta}(t) \equiv \frac{\theta(t) \exp(-k_{\alpha} t) + \theta(-t) \exp(k_{\beta} t)}{k_{\alpha} + k_{\beta}} \quad (\text{B7})$$

The population averaged autocorrelation considered in IIA is given by  $A(t) = \frac{1}{N} \sum_i C_{ii}(t)$ , which reads

$$A(t) = \frac{1}{N} \sum_{\alpha\beta} G_{\alpha\beta}(t) L_{\alpha\beta}, \quad (\text{B8})$$

where we defined the so-called overlap matrix

$$L_{\alpha\beta} = \sum_i V_{i\alpha} V_{i\beta} \sum_h V_{\alpha h}^{-1} V_{\beta h}^{-1} \quad (\text{B9})$$

which is a measure of how much different modes overlap in neuronal space. It is diagonal in the case  $\nu = 0$  of orthonormal  $V = O$ . For large number of neurons  $N$ ,  $L$  is self averaging, meaning  $L \sim \langle L \rangle_{O,G}$  apart from fluctuations of subleading order in  $N$ . We can therefore compute  $L$  in this limit using the methods exposed in A 4. The precise calculation is intricate and will be reported elsewhere. The result is

$$L_{\alpha\beta} = \frac{1 + \nu^2}{1 - \nu^2} \delta_{\beta,\alpha^*} - \frac{2}{N} \frac{\nu^2}{1 - \nu^2} \quad (\text{B10})$$

As commented in IIA, the first term is the only one present in the limit of orthonormal eigenvectors  $\nu \rightarrow 0$ , while the second term reflects a non-vanishing overlap between eigenvectors for any other  $\nu \neq 0$ . Eq. (9) in IIA is obtained by plugging Eq. (B10) into Eq. (B8) and taking the limit of the sum over eigenvalues to an integral over their probability density, with integration measure  $Dk \equiv p(k) dk$ .

## 2. Dimensionality

Let us recall the definition of the participation ratio for a generic covariance matrix  $C$

$$D \equiv \frac{(\text{Tr}[C])^2}{\text{Tr}[C^2]} \quad (\text{B11})$$

For the equal-time covariance,  $C$  corresponds to  $C(t=0)$  given by Eq. (B7), while for the long time-window covariance  $C$  corresponds to  $C(\omega=0)$  given by Eq. (B6).

*Equal-time covariance* As noted in IIB, for the equal-time covariance, the numerator  $(\text{Tr}[C])^2$  corresponds to  $A(t=0)^2$  given in Eq. (9), whose diverging behavior near criticality is discussed in Eq. (11). Using Eq. (B7) the expression for the denominator reads

$$\text{Tr}[C^2] = \frac{1}{N^2} \sum_{\alpha\beta\gamma\delta} G_{\alpha\beta}(t=0) G_{\gamma\delta}(t=0) L_{\alpha\beta\gamma\delta}^{(2)}, \quad (\text{B12})$$

where we defined the overlap tensor

$$L_{\alpha\beta\gamma\delta}^{(2)} = \sum_i V_{i\alpha} V_{i\gamma} \sum_j V_{j\beta} V_{j\delta} \sum_h V_{\alpha h}^{-1} V_{\beta h}^{-1} \sum_k V_{\gamma k}^{-1} V_{\delta k}^{-1} \quad (\text{B13})$$

Like  $L$ , also  $L^{(2)}$  is self averaging and can be computed with the same methods. The result is very lengthy and will be reported elsewhere. Here we only report the term that dominates in the diverging behavior of  $\text{Tr}[C^2]$  near criticality

$$L_{\alpha\beta\gamma\delta}^{(2)} \sim \left( \frac{1 + \nu^2}{1 - \nu^2} \right)^2 \delta_{\beta,\alpha^*} \delta_{\gamma,\alpha^*} \delta_{\delta,\alpha}$$

which plugged into Eq. (B12) gives Eq. (16) in IIB.

*Long time-window covariance* The reasoning for the long time-window covariance is completely analogous. By comparing Eq. (B7) with Eq. (B6) we notice that one simply needs to replace  $G_{\alpha\beta}(t=0) \rightarrow G_{\alpha\beta}(\omega=0)$ . This leads to the results given in IIB. Notice that, while  $G_{\alpha\alpha^*}(t=0) = \frac{1}{\text{Re}k_\alpha}$ , instead  $G_{\alpha\alpha^*}(\omega=0) = \frac{1}{|k_\alpha|^2}$ , so the relevant direction along which to approach criticality is the radial one, instead of the real axis.

## 3. Principal components spectrum

From Eq. (B7) and Eq. (B6) we immediately see that for  $\nu = 0$  the eigenvalues  $c_\alpha$  of the equal time or long time-window covariance are, respectively,  $G_{\alpha\alpha^*}(t=0) = \frac{1}{\text{Re}k_\alpha}$  and  $G_{\alpha\alpha^*}(\omega=0) = \frac{1}{|k_\alpha|^2}$ . Indeed, for  $\nu = 0$  the eigenvectors are orthonormal and so the term  $\sum_h V_{\alpha h}^{-1} V_{\beta h}^{-1} = \delta_{\beta,\alpha^*}$ . From this observation follow the results discussed in IIC.

- 
- [1] M. Mehta, *Random matrices*, vol. 142 of *Pure and Applied Mathematics* (Elsevier Ltd., 2004), 3rd ed.
  - [2] G. Akemann, J. Baik, and P. Di Francesco, *The Oxford Handbook of Random Matrix Theory* (Oxford University Press, 2015), URL <https://doi.org/10.1093/oxfordhb/9780198744191.001.0001>.
  - [3] E. P. Wigner, Ann. Math. **62**, 548 (1955).
  - [4] H. Sompolinsky, A. Crisanti, and H. J. Sommers, Phys. Rev. Lett. **61**, 259 (1988).
  - [5] C. van Vreeswijk and H. Sompolinsky, Science **274**, 1724 (1996).
  - [6] D. J. Amit and N. Brunel, Cereb. Cortex **7**, 237 (1997).
  - [7] N. Brunel, J. Comput. Neurosci. **8**, 183 (2000).
  - [8] Y. Hu, J. Trousdale, K. Josić, and E. Shea-Brown, J. Stat. Mech. Theory Exp. **2013**, P03012 (2013).
  - [9] Y. Hu and H. Sompolinsky, PLOS Computational Biology **18**, 1 (2022).
  - [10] S. Song, P. Sjöström, M. Reigl, S. Nelson, and D. Chklovskii, PLOS Biol. **3**, e68 (2005).
  - [11] J. M. Beggs and D. Plenz, J. Neurosci. **23**, 11167 (2003).
  - [12] C. Haldeman and J. M. Beggs, Phys. Rev. Lett. **94**, 058101 (2005).
  - [13] A. J. Fontenele, N. A. P. de Vasconcelos, T. Feliciano, L. A. A. Aguiar, C. Soares-Cunha, B. Coimbra, L. Dalla Porta, S. Ribeiro, A. J. Rodrigues, N. Sousa, et al., Phys. Rev. Lett. **122**, 208101 (2019).

- [14] L. Meshulam, J. L. Gauthier, C. D. Brody, D. W. Tank, and W. Bialek, Phys. Rev. Lett. **123**, 178103 (2019).
- [15] P. T. Sadtler, K. M. Quick, M. D. Golub, S. M. Chase, S. I. Ryu, E. C. Tyler-Kabara, B. M. Yu, and A. P. Batista, Nature **512**, 423 (2014), ISSN 1476-4687, number: 7515 Publisher: Nature Publishing Group.
- [16] J. A. Gallego, M. G. Perich, S. N. Naufel, C. Ethier, S. A. Solla, and L. E. Miller, Nat. Commun. **9**, 1 (2018).
- [17] C. Stringer, M. Pachitariu, N. Steinmetz, M. Carandini, and K. D. Harris, Nature **571**, 361 (2019).
- [18] D. Grytskyy, T. Tetzlaff, M. Diesmann, and M. Helias, Front. Comput. Neurosci. **7**, 131 (2013).
- [19] J. Trousdale, Y. Hu, E. Shea-Brown, and K. Josic, PLOS Comput. Biol. **8**, e1002408 (2012).
- [20] H. Sommers, A. Crisanti, H. Sompolinsky, and Y. Stein, Phys. Rev. Lett. **60**, 1895 (1988).
- [21] D. R. Chialvo, Nat. Phys. **6**, 744 (2010), ISSN 1745-2481, number: 10 Publisher: Nature Publishing Group.
- [22] C. G. Langton, Physica D **42**, 12 (1990).
- [23] N. Bertschinger and T. Natschlager, Neural Comput. **16**, 1413 (2004).
- [24] K. G. Wilson, Rev. Mod. Phys. **47**, 773 (1975).
- [25] P. C. Hohenberg and B. I. Halperin, Rev. Mod. Phys. **49**, 435 (1977).
- [26] U. C. Taeuber, *Critical dynamics: a field theory approach to equilibrium and non-equilibrium scaling behavior* (Cambridge University Press, 2014), ISBN 9780521842235.
- [27] J. D. Semedo, A. Zandvakili, C. K. Machens, M. Y. Byron, and A. Kohn, Neuron **102**, 249 (2019).
- [28] S. Recanatesi, G. K. Ocker, M. A. Buice, and E. Shea-Brown, PLOS Comput. Biol. **15**, 1 (2019).
- [29] D. Dahmen, S. Recanatesi, X. Jia, G. K. Ocker, L. Campagnola, T. Jarsky, S. Seeman, M. Helias, and E. Shea-Brown, BioRxiv (2022).
- [30] M. A. Munoz, R. Dickman, A. Vespignani, and S. Zapperi, Phys. Rev. E **59**, 6175 (1999).
- [31] S. Bradde and W. Bialek, J. Stat. Phys. **167**, 462 (2017), ISSN 1572-9613.
- [32] J. Schuecker, S. Goedeke, and M. Helias, Phys. Rev. X **8**, 041029 (2018).
- [33] L. Tiberi, J. Stappmanns, T. Luu, D. Dahmen, and M. Helias, Phys. Rev. Lett. **128** (2022).
- [34] K. Rajan and L. F. Abbott, Phys. Rev. Lett. **97**, 188104 (2006).
- [35] M. Helias and D. Dahmen, *Statistical Field Theory for Neural Networks* (Springer International Publishing, 2020).
- [36] D. Weingarten, Journal of Mathematical Physics **19**, 999 (1978), ISSN 0022-2488, publisher: American Institute of Physics.
- [37] B. Collins and P. Snady, Communications in Mathematical Physics **264**, 773 (2006), ISSN 1432-0916.
- [38] S. Matsumoto, The Ramanujan Journal **26**, 69 (2011), ISSN 1572-9303.



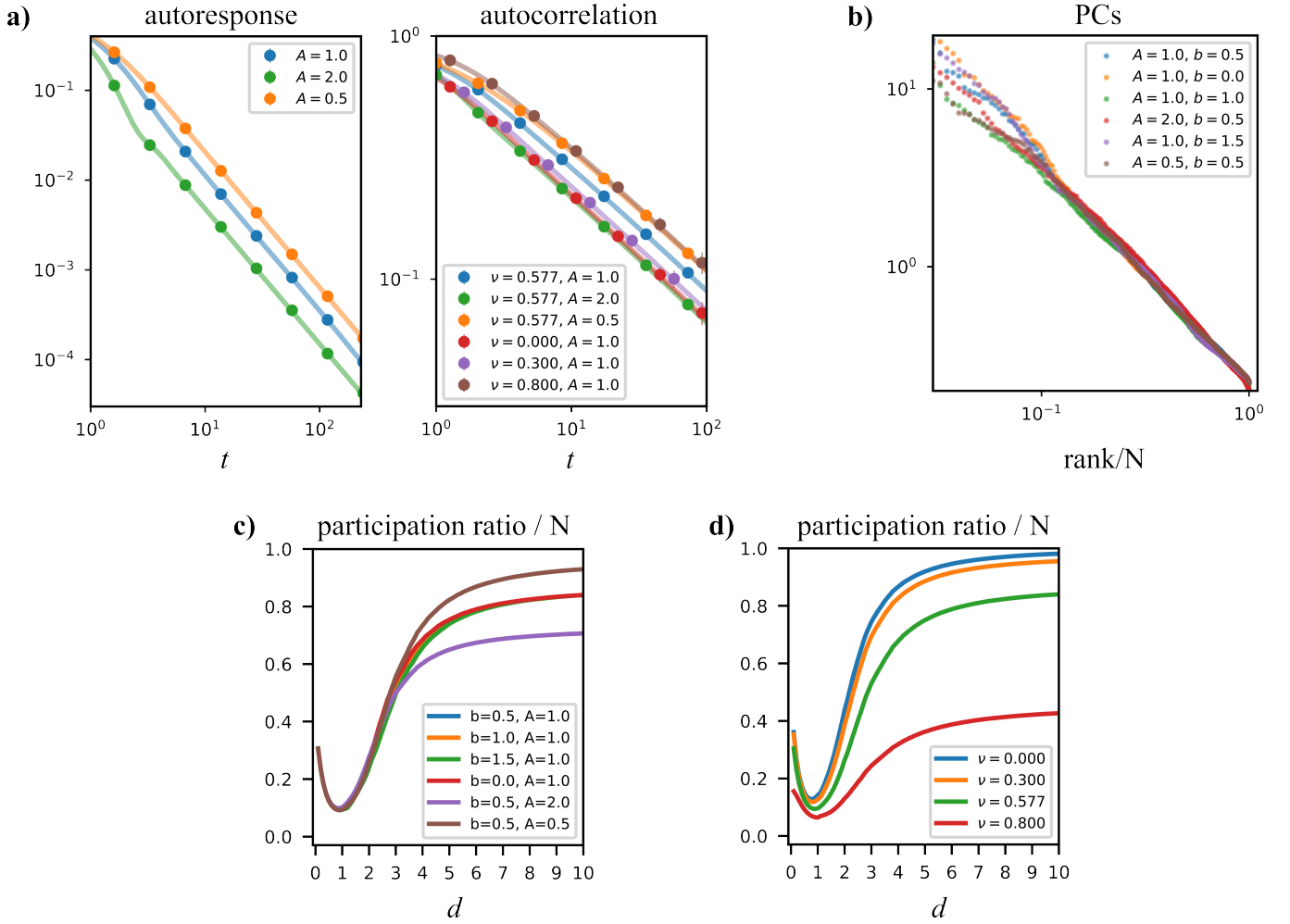


Figure S1. Irrelevance of details in the eigenvalue distribution shape and/or the degree of non-normality. (a) Autoresponse and autocorrelation, for  $d = 1.5$ . Shown for varying stretching  $A$  of the eigenvalue distribution along the imaginary axis (cfr. Eq. (12)) and for varying degree of non-normality  $\nu$  (autocorrelation only). Even if these parameters vary, the power-law decay of both functions is only controlled by  $d$  and remains the same. Markers: simulation; lines: theory. Other parameters:  $b = 1.0$ ,  $N = 10^2$ . (b) Principal component spectrum of the equal-time covariance, for  $d = 1.0$ . Shown for varying  $A$  and varying  $b$ , controlling the boundary of the eigenvalue distribution (cfr. Eq. (12)). Even if these parameters vary, the power-law decay is only controlled by  $d$  and remains the same. Other parameters:  $\nu = 1/\sqrt{3}$ ,  $N = 4 \cdot 10^2$ ,  $\delta = 0.01$ . (c) Dimensionality of the equal-time covariance, for  $\delta = 0.01$ . Shown for varying  $A$  and  $b$ . Even if these parameter vary, the transition from high to low dimensionality has the same characteristic. A clear minimum is present at  $d \sim 1$ . In the region  $d < 2$  where dimensionality  $\rightarrow 0$  as  $\delta \rightarrow 0$ , all curves coincide. For  $d > 2$ , the finite limit-value taken by dimensionality can change quantitatively. Lines: theory. Other parameters:  $\nu = 1/\sqrt{3}$ . (d) Dimensionality of the equal-time covariance, for  $\delta = 0.01$ . Shown for varying  $\nu$ . Though  $\nu$  affects dimensionality quantitatively, the transition from high to low dimensionality has the same characteristic, with a clear minimum, present at  $d \sim 1$ . Lines: theory. Other parameters:  $A = 1$ ,  $b = 0.5$ .

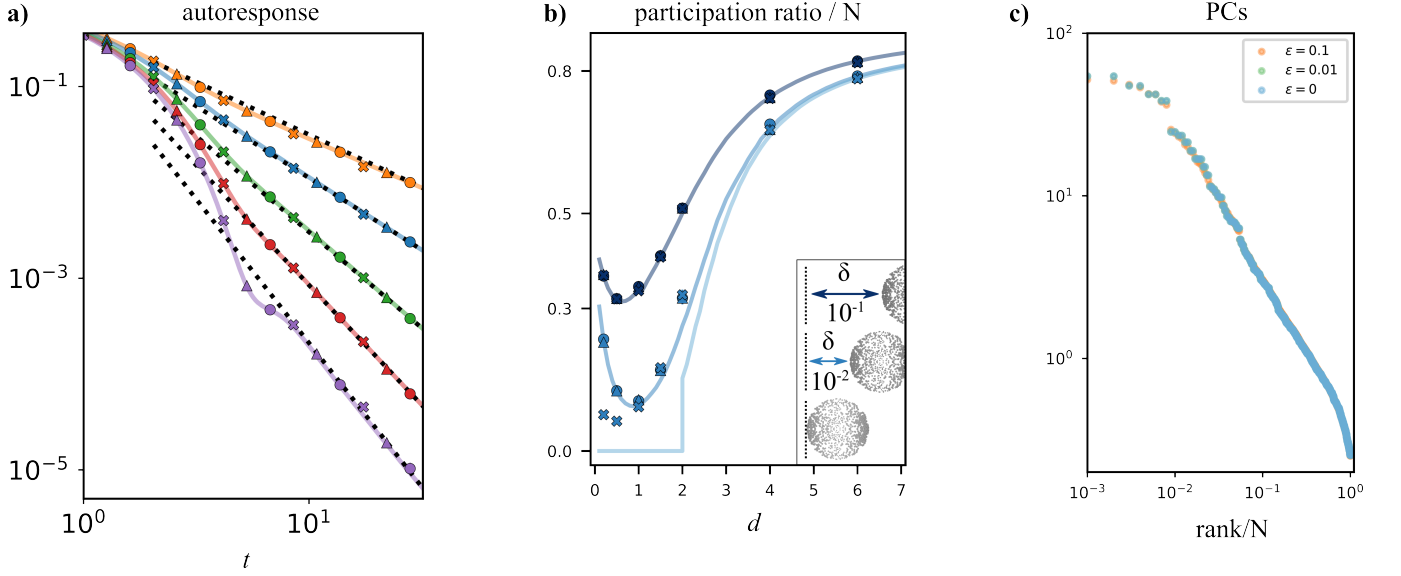


Figure S2. Robustness of the dynamics to perturbations of the connectivity. (a) Analogous to Fig. 3(b). The autoresponse is shown for fixed  $b = 1$  and varying  $d$  (colors). Solid curves: theory; markers: simulations; dashed, black lines: power-law decay with exponent  $d$ . In addition to the unperturbed connectivity (circles), we show simulations where the connectivity is subject to a 1% (triangles) and 10% (stars) perturbation (cfr. III C). Note how the results are not altered appreciably by the perturbation. (b) Analogous to II B(a). The participation ratio of the equal-time covariance is shown, as a function of  $d$ . Curves in lighter blue correspond to decreasing values of  $\delta$  (see inset). Solid curves: theory; markers: simulations. Again, in addition to the unperturbed connectivity (circles), we show simulations where the connectivity is subject to a 1% (triangles) and 10% (stars). Note how the results are not altered appreciably by the perturbation. The only exception is for  $d < d_c = 1$ , at which the dynamics become sensitive to the 10% perturbation, if the system is very close to criticality ( $\delta = 10^{-2}$ ). Analogous result holds for the long time-window covariance. (c) Eigenvalues of the long time-window covariance plotted against their fractional rank. Case  $\nu = 1/\sqrt{3}$ ,  $d = 2$ . Shown for different strengths  $\epsilon$  of perturbation of the connectivity (legend). Note how the spectrum is not unaltered appreciably by the perturbation. Analogous results hold for the equal-time covariance.